JACS
JOURNAL OF THE AMERICAN CHEMICAL SOCIETY
Article
pubs.acs.org/JACS

Triangular Monometallic Cyanide Cluster Entrapped in Carbon Cage with Geometry-Dependent Molecular Magnetism

Fupin Liu,[†] Cong-Li Gao,[‡] Qingming Deng,[§] Xianjun Zhu,[†] Aram Kostanyan,[∥] Rasmus Westerström,[∥] Song Wang,[†] Yuan-Zhi Tan,[‡] Jun Tao,[‡] Su-Yuan Xie,*[,‡] Alexey A. Popov,*[,§] Thomas Greber,*[,∥] and Shangfeng Yang*[,†]

[†]Hefei National Laboratory for Physical Sciences at Microscale, Key Laboratory of Materials for Energy Conversion, Chinese Academy of Sciences, Department of Materials Science and Engineering, Synergetic Innovation Center of Quantum Information & Quantum Physics, University of Science and Technology of China (USTC), Hefei 230026, China

[‡]State Key Laboratory of Physical Chemistry of Solid Surfaces, iChEM (Collaborative Innovation Center of Chemistry for Energy Materials), Department of Chemistry, College of Chemistry and Chemical Engineering, Xiamen University, Xiamen 361005, China

[§]Leibniz Institute for Solid State and Materials Research Dresden, Helmholtzstrasse 20, Dresden 01069, Germany

[∥]Physik-Institut, Universität Zürich, Winterthurerstrasse 190, CH-8057 Zürich, Switzerland

Supporting Information

ABSTRACT: Clusterfullerenes are capable of entrapping a variety of metal clusters within carbon cage, for which the entrapped metal cluster generally keeps its geometric structure (e.g., bond distance and angle) upon changing the isomeric structure of fullerene cage, and whether the properties of the entrapped metal cluster is geometry-dependent remains unclear. Herein we report an unusual triangular monometallic cluster entrapped in fullerene cage by isolating several novel terbium cyanide clusterfullerenes (TbNC@C_{82}) with different cage isomeric structures. Upon varying the isomeric structure of C_{82} cage from $C_2(5)$ to $C_s(6)$ and to $C_{2v}(9)$, the entrapped triangular TbNC cluster exhibits significant distortions as evidenced by the changes of Tb−C(N) and C−N bond distances and variation of the Tb−C(N)−N(C) angle by up to 20°, revealing that the geometric structure of the entrapped triangular TbNC cluster is variable. All three TbNC@C_{82} molecules are found to be single-ion magnets, and the change of the geometric structure of TbNC cluster directly leads to the alternation of the magnetic relaxation time of the corresponding TbNC@C_{82} clusterfullerene.

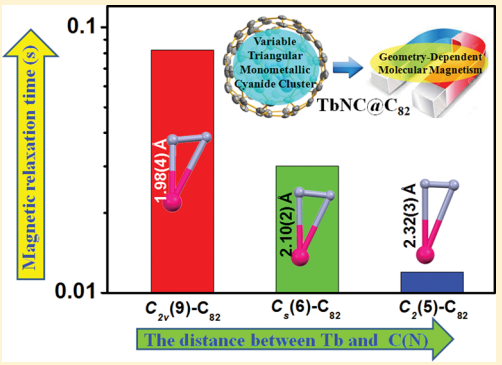

INTRODUCTION

Fullerene has a hollow interior, able to entrap versatile species such as atoms, ions and metal clusters in the form of endohedral fullerenes.[1−4] During the past two decades, comprehensive studies on different types of endohedral fullerenes reveal that the interplay between the size/shape of the entrapped species and the fullerene cage plays an important role on the stabilization of endohedral fullerenes.[1−11] Due to the charge transfer from the entrapped species to the outer fullerene cage, such unstable species as the charged metal clusters can be stabilized to form endohedral clusterfullerenes.[9] Among all endohedral fullerenes reported up to now, clusterfullerenes exhibit the largest diversity of the entrapped species, including metal nitrides,[1,6] carbides,[11−13] oxides,[14] sulfides,[15] hydrocarbide,[16] carbonitride,[17] and a unique $TiLu_2C$ cluster with a central μ_3-C atom and double Ti = C bond reported recently.[18] Despite the recent advance on clusterfullerenes focusing on searching for new structures, the dependence of the geometric structure of the entrapped metal cluster on the outer fullerene cage remains unclear, and limited reports revealed that the entrapped metal cluster within fullerene cage generally keeps its geometric structure (e.g., bond distance and angle) upon changing the isomeric structure of fullerene cage. In few cases, even though the geometric structure of the entrapped metal cluster altered, the central nonmetal ion remains in the center of the cage and the change of the bond distance within the metal cluster was typically negligible when the cage isomeric structure changed. For instance, X-ray crystallographic studies of two isomers of scandium (Sc)-based sulfide clusterfullerenes $Sc_2S@C_{82}$ revealed that, upon changing its cage isomeric structure from $C_s(6)$-C_{82} to $C_{3v}(8)$-C_{82}, the change on the Sc−S bond distance within the Sc_2S cluster is negligible (<0.08 Å) although the Sc−S−Sc angle decreases from 114° to 97°.[19] Likewise, for the well-known Sc-based nitride clusterfullerenes $Sc_3N@C_{80}$ (I_h, D_{5h}), variation of the cage isomeric structure from I_h-C_{80} to D_{5h}-C_{80} resulted in no change on the planar triangular geometry of the Sc_3N cluster despite of a small variation of the averaged Sc−N bond distance of less than 0.05 Å.[1,20]

Received: September 5, 2016
Published: October 18, 2016

DOI: 10.1021/jacs.6b09329
J. Am. Chem. Soc. 2016, 138, 14764−14771

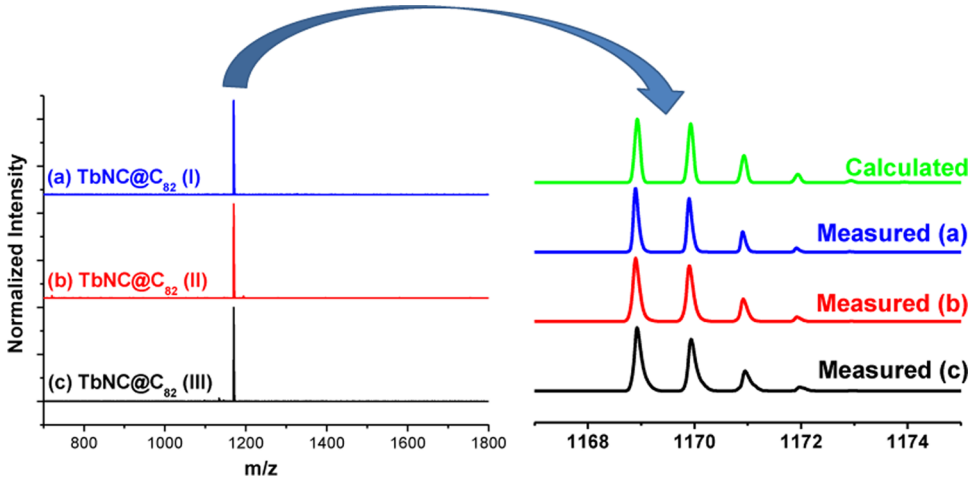

Figure 1. Negative-ion LD-TOF mass spectrum of the purified TbNC@C_{82} (I–III). Insets: measured and calculated isotopic distributions of TbNC@C_{82}.

Because of the intramolecular charge transfer from the entrapped metal cluster to the outer fullerene cage, clusterfullerene exhibits unique electronic, physical and chemical properties.[1−4] In particular, the magnetic properties of clusterfullerenes appear quite intriguing and complicated because of the exchange interactions among multiple paramagnetic lanthanide ions entrapped.[1−4,21] Recently a few clusterfullerenes including metal nitride clusterfullerenes $Ln_xSc_{3-x}N@C_{80}$ (Ln = Dy, Ho, x = 1, 2)[22−25] and carbide clusterfullerene $Dy_2TiC@C_{80}$ (ref 26) were found to behave as single molecule magnets (SMMs) or more specifically single-ion magnets (SIMs), which are SMMs containing only a single magnetic ion,[27−34] showing potential applications in spintronics, quantum computing and high-density storage devices.[22−34] They all have a central nonmagnetic ion (N or C) that imposes a strong ligand field, which provides the anisotropy for the single molecule magnetism. In contrast to the well-known conventional SIMs based on coordination compounds, endohedral fullerene provides a truly individual molecular system as a kind of ideal SIM with a well-isolated metal ion anchored in a certain position.[1,22−26] Noteworthy, since for those known clusterfullerenes the entrapped metal cluster within fullerene cage generally keeps its geometric structure when the cage isomeric structure changes, the central nonmetal ion remains in the center of the cage and it is not clear whether the magnetic properties of clusterfullerene SIMs would change upon altering the geometric structure of the entrapped cluster and consequently its coordination to the diamagnetic cage.

Herein, we report on an unusual triangular terbium cyanide (TbNC) cluster entrapped in fullerene cage on the basis of isolating several novel Tb-based metal cyanide clusterfullerene including three isomers of TbNC@C_{82}. Upon varying the isomeric structure of C_{82} cage from $C_2(5)$, $C_s(6)$ to $C_{2v}(9)$, the triangular TbNC cluster distorts as evidenced by the dramatic change of the Tb−N(C)/C−N bond length and the Tb−C(N)−N(C) angle. Furthermore, such geometric structural changes of the entrapped TbNC cluster dictated by fullerene cage are found to directly lead to the change of magnetic relaxation times of the corresponding metal cyanide clusterfullerenes.

RESULTS AND DISCUSSION

Synthesis, Isolation, and Cage Isomeric Structures of Three Isomers of TbNC@C_{82}. As an entrant of clusterfullerene family, metal cyanide clusterfullerene (CYCF) discovered recently represents the first endohedral fullerene entrapping a monometallic cluster.[35] Up to now only two CYCFs have been isolated which are both based on C_{82} cage, including YNC@$C_s(6)$-C_{82} and TbNC@$C_2(5)$-C_{82}, and a striking structural feature of them is that the entrapped MNC (M = Y, Tb) cluster takes a triangular geometry.[35,36] Such a triangular geometry of the MNC cluster is rather unusual because it has been well-known that the traditional inorganic metal cyanide compounds or cyano coordination complexes exhibit linear structures, while a bent metal−C−N structure was observed only when the C and N atoms within the CN^- ligand were coordinated with two metal atoms.[37−39] Thus, the triangular geometry of the MNC cluster can be stabilized only in the confined space of fullerene cage.[35,36] Moreover, the C−N bond length found in YNC@$C_s(6)$-C_{82} and TbNC@$C_2(5)$-C_{82} is only 0.935 and 0.94(5) Å, respectively, which is smaller by at least 0.17 Å than those of the reported C−N triple bonds in traditional inorganic metal cyanides and cyano coordination complexes as well as the organic nitrile compounds.[40−42] The unusual triangular geometry and small C−N bond length of the MNC cluster within the reported MNC@C_{82} (M = Y, Tb) suggest that the MNC cluster is highly strained in the confined space of C_{82} cage.[35] Thus, we are stimulated to address whether the strained MNC cluster within CYCF is rigid like those within other known clusterfullerenes.

The synthesis procedure of three isomers of TbNC@C_{82} (labeled as I–III) by a modified Krätschmer−Huffman DC arc discharge method involving nitrogen gas (N_2) is similar to that of YNC@$C_s(6)$-C_{82} we reported recently.[35] An optimized condition (the molar ratio of Tb:C = 1:15; discharging atmosphere: 400 mbar He mixed with 10 mbar N_2) was used.[36] TbNC@C_{82} (I–III) were successfully isolated from fraction **A**/**A′** by a two-step HPLC (see Supporting Information S1 for details). To ensure the high purity of the isolated TbNC@C_{82} (I–III), we carried out laser desorption time-of-flight (LD-TOF) mass spectroscopy (MS), showing a single mass peak at m/z = 1169 for which the isotopic distribution analysis shows a good coincidence with the calculated one (Figure 1).

DOI: 10.1021/jacs.6b09329
J. Am. Chem. Soc. 2016, 138, 14764−14771

The molecular structures of the isolated TbNC@C_{82} (I–III) were determined unambiguously by X-ray crystallographic study based on their corresponding cocrystals with Ni^{II}(OEP) (OEP = octaethylporphyrin).[43−46] The cage structure of TbNC@C_{82} (I, C_2(5)) has been reported very recently.[36] Figures 2a and 2c show the relative orientations of TbNC@C_{82}

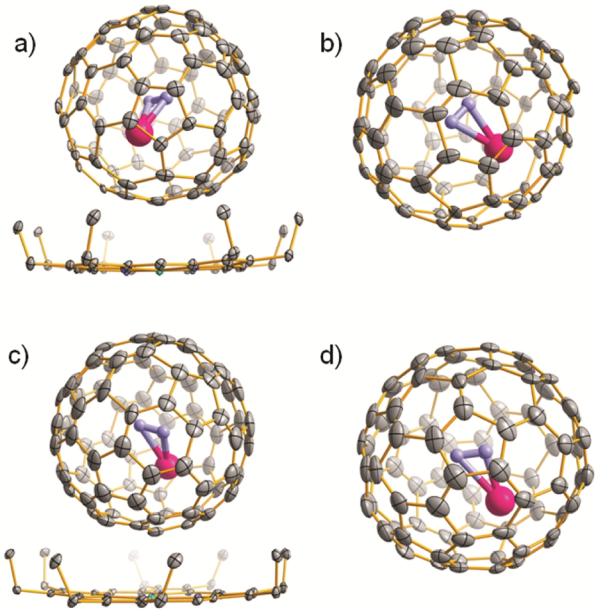

Figure 2. Single crystal X-ray structures of TbNC@C_{82} (C_s(6), C_{2v}(9)). The structures of TbNC@C_s(6)-C_{82}·Ni^{II}(OEP)·2(C_6H_6) (a) and TbNC@C_{2v}(9)-C_{82}·Ni^{II}(OEP)·2(C_6H_6) (c) are shown with only the predominant Tb (Tb1) positions, and solvent benzene molecules and hydrogen atoms are omitted for clarity. The structures of TbNC@C_s(6)-C_{82} and TbNC@C_{2v}(9)-C_{82} with the major TbNC clusters are illustrated in (b) and (d), respectively.

(II, C_s(6)), TbNC@C_{82} (III, C_{2v}(9)) and the Ni^{II}(OEP) molecules in TbNC@C_s(6)-C_{82}·Ni^{II}(OEP)·2(C_6H_6) and TbNC@C_{2v}(9)-C_{82}·Ni^{II}(OEP)·2(C_6H_6) cocrystals, respectively. Only one orientation of the fullerene cage together with the major site of TbNC cluster is shown in the drawings for clarity. For both cases of TbNC@C_s(6)-C_{82} and TbNC@C_{2v}(9)-C_{82}, the asymmetric unit cell of the cocrystal contains a half of the Ni^{II}(OEP) molecule and two halves of the C_s(6)-C_{82}/C_{2v}(9)-C_{82} cage. The crystallographic mirror bisects N 2p, N 3p, Ni 1p, C83(N1), N1(C83) and is perpendicular to the paper plane (see Supporting Information Figures S4A and S5A). The fully ordered Ni^{II}(OEP) molecule is present perpendicular to the crystal mirror plane that bisects the Ni 1p, N 2p and N 3p, so the intact molecule is generated by combining the existing half molecule with its mirror image, and a complete C_s(6)-C_{82}/C_{2v}(9)-C_{82} cage is generated by combining one of the halves of the fullerene cage with the other for which both have an occupancy of 0.50. The nearest Ni-cage contact is 2.826(12) (C16a-Ni 1p) and 2.80(3) Å (C09a-Ni 1p) for TbNC@C_s(6)-C_{82}·Ni^{II}(OEP)·2(C_6H_6) and TbNC@C_{2v}(9)-C_{82}·Ni^{II}(OEP)·2(C_6H_6) cocrystals, respectively, which are comparable to that observed in the reported TbNC@C_2(5)-C_{82}·Ni^{II}(OEP)·2(C_6H_6) cocrystal.[36]

Geometric Structures of TbNC Clusters within TbNC@C_{82} (C_2(5), C_s(6), C_{2v}(9)). As commonly observed in clusterfullerenes including the reported YNC@C_s(6)-C_{82} and TbNC@C_2(5)-C_{82} CYCFs,[35,36] the entrapped TbNC clusters within TbNC@C_{82} (C_s(6), C_{2v}(9)) all exhibit disorders. As a result, as many as 12 and 16 Tb sites are refined for TbNC@C_s(6)-C_{82} and TbNC@C_{2v}(9)-C_{82}, respectively (see Supporting Information Figures S4–S5). For the NC moiety, positional disorder of the N and C atoms was not detected according to the present X-ray data, while it may exist as conjectured from the geometries of different Tb sites. Furthermore, the detected NC moiety locates on the crystal mirror plane, but distinguishing nitrogen and carbon atoms is challenging because of their similarities on the atomic size and scattering power.[17,36,47] Although there exists severe disorders for the encapsulated Tb atom, the major site Tb1 occupied a much higher probability than the other minor sites, i.e., 0.274(3) and 0.233(3) for TbNC@C_s(6)-C_{82} and TbNC@C_{2v}(9)-C_{82}, respectively (see Supporting Information Figures S4–S5), so we take Tb1 site as the representative TbNC cluster in the following discussion. Noteworthy, similar to the reported YNC@C_s(6)-C_{82} and TbNC@C_2(5)-C_{82} CYCFs, the entrapped TbNC cluster in C_s(6)-C_{82}/C_{2v}(9)-C_{82} cage takes a triangular geometry (see Figures 2 and 3b,c), which is dramatically different from the linear structures commonly found in traditional metal cyanide complexes.[37−41]

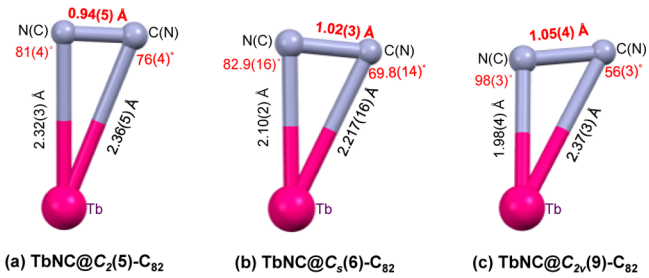

Figure 3. Comparison of the geometric structures of the TbNC clusters within TbNC@C_{82} (C_2(5), C_s(6), C_{2v}(9)). The structures of the major TbNC clusters within C_2(5)-C_{82} (a, ref 36), C_s(6)-C_{82} (b) and C_{2v}(9)-C_{82} (c) with X-ray determined bond lengths and bond angles are shown.

The geometric structure of the entrapped cluster within a clusterfullerene is crucial for the intramolecular interaction between the cluster and the outer carbon cage which determines the stability of specific cage isomer.[3,9] For the same type of clusterfullerenes, the geometric structure of the entrapped cluster can be also regarded as a measure of the internal strain within the confined space of carbon cage.[48] For TbNC@C_{82} (C_2(5), C_s(6), C_{2v}(9)), when the cage isomeric structure changes from C_2(5), C_s(6) to C_{2v}(9), the distance of the shorter Tb1–C83(N1)/Tb–N1(C83) bond decreases dramatically from 2.32(3), 2.10(2) to 1.98(4) Å, whereas that of the longer Tb1–N1(C83)/Tb–C83(N1) bond changes from 2.36(5), 2.217(16) to 2.37(3) Å. As a result, the triangular TbNC cluster exhibits obvious distortions with the Tb–C(N)–N(C) angle varying by up to 20° (see Figure 3a–c). This suggests that, dramatically different to the cases of metal sulfide and nitride within the corresponding clusterfullerenes, the geometric structure of the entrapped TbNC cluster is dictated by the fullerene cage.

The dramatic geometric change of the entrapped TbNC cluster within TbNC@C_{82} (C_2(5), C_s(6), C_{2v}(9)) is further confirmed in terms of the C–N bond length. Interestingly, when the cage isomeric structure of TbNC@C_{82} changes from

DOI: 10.1021/jacs.6b09329
J. Am. Chem. Soc. 2016, 138, 14764–14771

$C_2(5)$, $C_s(6)$ to $C_{2v}(9)$, the C−N bond length increases gradually from 0.94(5), 1.02(3) to 1.05(4) Å by neglecting the *esd*'s (see Figure 3a−c). Such a change of the C−N bond length indicates further the distortion of the TbNC cluster within C_{82} cage. In fact, the C−N bond length within TbNC@$C_{2v}(9)$-C_{82} becomes more close to those of the reported C−N triple bonds in traditional cyanide/nitrile compounds and cyano coordination complexes (1.12−1.17 Å, see Supporting Information Table S4 for details).[39−42] The change of the C−N bond length along with the distortion of the TbNC cluster discussed above reveal that the entrapped TbNC cluster is variable by altering the outer fullerene cage. To our knowledge, this phenomenon has never been reported for other known endohedral fullerenes.

The unprecedented variability of the entrapped cluster within fullerene cage is rather surprising because the geometric structure change of the entrapped metal cluster within clusterfullerenes would have sensitively affected the stability of the clusterfullerene. While this phenomenon has not been fully understood yet, a plausible interpretation is that, upon varying the cage isomeric structure from $C_2(5)$, $C_s(6)$ to $C_{2v}(9)$, the coordination bonding between Tb metal atom and CN^- ligand would be weakened as a result of the strengthening of the Tb-cage interaction inferred from the decrease of the average distance between Tb and the nearest carbon atoms of the C_{82} cage (see Supporting Information Figure S6 and Table S3).

Electronic Properties of TbNC@C_{82} ($C_2(5)$, $C_s(6)$, $C_{2v}(9)$). Figure 4 shows the UV−vis−NIR absorption spectra of

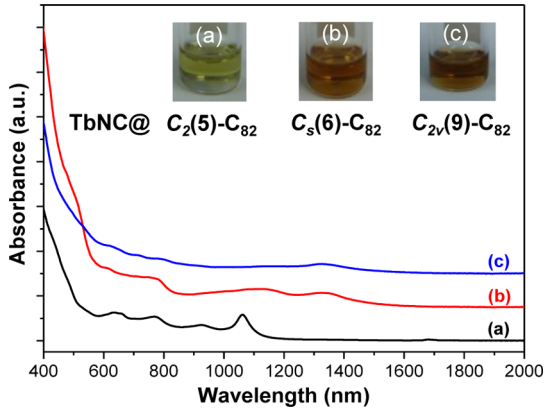

Figure 4. UV−vis−NIR spectra and photographs of TbNC@C_{82} ($C_2(5)$, $C_s(6)$, $C_{2v}(9)$) dissolved in CS_2. Insets: Photographs of the corresponding solutions in toluene.

TbNC@C_{82} ($C_2(5)$, $C_s(6)$, $C_{2v}(9)$) dissolved in CS_2, and their characteristic absorption data are summarized in Supplementary Table S6 and compared in Supporting Information S4. For TbNC@$C_s(6)$-C_{82} (see curve b, Figure 4), its overall absorption spectrum and all of the absorption features, including the characteristic absorption peaks, the optical band gap ($\Delta E_{gap,optical}$) and color of toluene solution of TbNC@$C_s(6)$-C_{82} are almost identical to those of YNC@$C_s(6)$-C_{82} with the same $C_s(6)$-C_{82} cage (see Supporting Information Figure S8),[35] confirming that the electronic absorptions of endohedral fullerenes are predominantly due to $\pi-\pi^*$ carbon cage transitions and depend on the cage isomeric structure.[3] With respect to TbNC@$C_{2v}(9)$-C_{82} (see curve c, Figure 4), its electronic absorption spectrum is less featured compared to those of TbNC@$C_2(5)$-C_{82} (ref 36) and TbNC@$C_s(6)$-C_{82}, while its $\Delta E_{gap,optical}$ (0.70 eV) is the smallest among the three isomers of TbNC@C_{82} (see Supporting Information Table S6).

Figure 5 presents the cyclic voltammograms of TbNC@C_{82} ($C_2(5)$, $C_s(6)$, $C_{2v}(9)$) measured in *o*-dichlorobenzene (*o*-DCB) with tetrabutylammonium hexafluorophosphate ($TBAPF_6$) as supporting electrolyte. The characteristic redox potentials are summarized in Table 1, which includes those of other analogous C_{82}-based endohedral fullerenes for comparison. TbNC@$C_s(6)$-C_{82} exhibits one reversible oxidation step with a half-wave potential ($E_{1/2}$) at 0.55 V in the anodic region. On the other hand, in the cathodic region, TbNC@$C_s(6)$-C_{82} shows four reversible reduction steps with $E_{1/2}$ at −0.59, −0.84, −1.77, −1.92 V, respectively (see Supporting Information Figure S9). Obviously, both the oxidation and the reduction potentials of TbNC@$C_s(6)$-C_{82} are nearly identical to those of YNC@$C_s(6)$-C_{82} (see Table 1).[35] Likewise, for TbNC@$C_{2v}(9)$-C_{82}, one reversible oxidation step with an $E_{1/2}$ at 0.55 V, which is shifted positively compared with those of TbNC@$C_2(5)$-C_{82} (ref 26) and TbNC@$C_s(9)$-C_{82}, and four reversible reduction steps for TbNC@$C_{2v}(9)$-C_{82} in the cathodic region were detected with $E_{1/2}$ at −0.46, −0.81, −1.78, −1.96 V, respectively (see Supporting Figure S10). Interestingly, while the $E_{1/2}$ of the first reduction potential shifts positively from TbNC@$C_2(5)$-C_{82} to TbNC@$C_s(9)$-C_{82} and to TbNC@$C_{2v}(9)$-C_{82}, their first oxidation potential experiences only a slight change (0.50−0.56 V), thus their electrochemical gaps ($\Delta E_{gap,ec}$) decrease gradually from TbNC@$C_2(5)$-C_{82} (1.38 V) to TbNC@$C_s(9)$-C_{82} (1.14 V) and to TbNC@$C_{2v}(9)$-C_{82} (1.07 V) (see Table 1). Such a change on $\Delta E_{gap,EC}$ is consistent with the change of their optical band gap ($\Delta E_{gap,optical}$) as discussed above. DFT calculations show that the frontier molecular orbitals of TbNC@C_{82} ($C_2(5)$, $C_s(6)$, $C_{2v}(9)$) are predominantly localized on the carbon cage (see Supporting Information Figure S7), hence TbNC@C_{82} ($C_2(5)$, $C_s(6)$, $C_{2v}(9)$) exhibit pronounced similarity in their redox potentials (specifically the reduction potentials) to those of the corresponding divalent metal-based monometallofullerene Yb@C_{82} isomers (see Table 1).[49] Furthermore, TbNC@C_{82} ($C_2(5)$, $C_s(6)$, $C_{2v}(9)$) all show a large separation (0.58−0.93

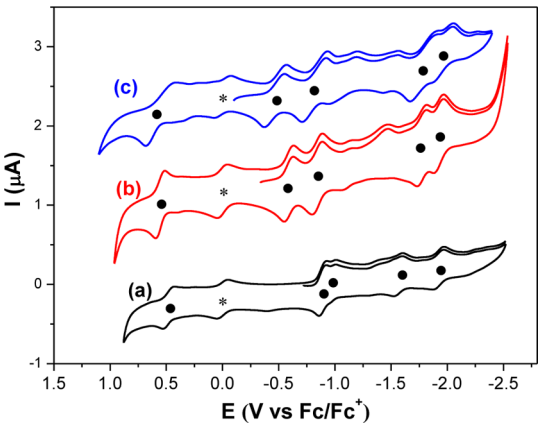

Figure 5. Cyclic voltammograms of TbNC@$C_2(5)$-C_{82} (a), TbNC@$C_s(6)$-C_{82} (b), and TbNC@$C_{2v}(9)$-C_{82} (c) measured in *o*-DCB solution. Ferrocene (Fc) was added as the internal standard, $TBAPF_6$ as supporting electrolyte, scan rate: 100 $mV \cdot s^{-1}$. The half-wave potentials ($E_{1/2}$) of each redox step are marked with a solid dot to aid comparison. The asterisk labels the oxidation peak of ferrocene.

DOI: 10.1021/jacs.6b09329
J. Am. Chem. Soc. 2016, 138, 14764−14771

Table 1. Redox Potentials (V vs Fc^+/Fc) and Electrochemical Gaps ($\Delta E_{gap,ec}$) of TbNC@C_{82} ($C_2(5)$, $C_s(6)$, $C_{2v}(9)$)[a]

	$E_{1/2}$ (V vs Fc/Fc^+)						
	reduction steps (E_{red})				oxidation step (E_{ox})		
sample	first	second	third	fourth	first	$\Delta E_{gap,EC}$/V[b]	ref.
TbNC@$C_2(5)$-C_{82}	−0.88	−0.97	−1.55	−1.91	0.50	1.38	36
Yb@$C_2(5)$-C_{82}	−0.86	−0.98	−1.50	−1.87	0.38	1.24	49
TbNC@$C_s(6)$-C_{82}	−0.59	−0.84	−1.77	−1.92	0.55	1.14	this work
YNC@$C_s(6)$-C_{82}	−0.59	−0.84	−1.76	−1.92	0.56	1.15	35
Yb@$C_s(6)$-C_{82}	−0.62	−0.92	−1.81	−2.01	0.34	0.96	49
TbNC@$C_{2v}(9)$-C_{82}	−0.46	−0.81	−1.78	−1.96	0.55	1.07	this work
Yb@$C_{2v}(9)$-C_{82}	−0.46	−0.78	−1.60	−1.90	0.61	1.07	49

[a]Other reported C_{82}-based endohedral fullerenes were also added for comparison. [b]$\Delta E_{gap,EC} = E_{1/2,ox(1)} - E_{1/2,red(1)}$.

V) between the second and third reduction steps, suggesting that they all have closed-shell electronic configurations derived from the same electronic configuration, namely $[Tb^{3+}(NC)^-]^{2+}@[C_{82}]^{2-}$.[36]

Magnetic Properties of TbNC@C_{82} ($C_2(5)$, $C_s(6)$, $C_{2v}(9)$). Since the paramagnetism of the TbNC@C_{82} molecule is governed by the 4f electrons of the entrapped Tb ion, it is intriguing to investigate whether the geometric structure change of the TbNC cluster upon altering the cage isomeric structure affects the magnetism of the TbNC@C_{82} molecule. The monometallic nature of the $[TbNC]^{2+}$ cluster anchored within the carbon cage and the fact that the natural abundance of Tb is limited to a single isotope with a nuclear spin of 3/2 make TbNC@C_{82} an interesting model system to understand the underlying physics of its magnetization. Trivalent Tb (Tb^{3+}) has eight 4f electrons with a $^7F_6$ Hund ground state. The ligand field, which is mainly governed by the $(NC)^-$ ion, lifts the 13-fold degenerate ground state, and eventually enables single molecule magnetism. Figure 6 shows the normalized magnetizations of TbNC@C_{82} ($C_2(5)$, $C_s(6)$, $C_{2v}(9)$) versus the applied field temperature quotient $x = \mu_0 H/T$ measured by superconducting quantum interference device (SQUID) at seven temperatures between 1.8 and 10 K. The magnetization curves of the individual TbNC@C_{82} molecules scale with x, while TbNC@$C_{2v}(9)$-C_{82} shows the largest deviations among different temperatures in the order of ±2%. Deviations from a perfect scaling may be due to a weak ligand field splitting, the corresponding ground state excitations and other interactions that do not scale with $\mu_0 H/T$. The noncollinear magnetic moment model considers that magnetic moments $\pm \boldsymbol{\mu}$ distribute isotropically in space, where the maximum of the two possible projections of $\boldsymbol{\mu}$ along the external H-field contributes to the magnetization (ref 23). This model has two parameters ($|\boldsymbol{\mu}|$ and the number of Tb atoms) and can be fitted almost perfectly to the experimental magnetization data (see Supporting Information S6). Accordingly, the magnetic moments $|\boldsymbol{\mu}|$ of TbNC@$C_2(5)$-C_{82}, TbNC@$C_s(6)$-C_{82} and TbNC@$C_{2v}(9)$-C_{82} are determined to be 9.0, 9.1, and 10.2 μ_B, respectively. This allows the assignment of the Tb ground state to $J_z = \pm 6$, with $L_z = 3$ and $S_z = 3$ and a magnetic moment of 9 μ_B. The magnetic moments of TbNC@$C_2(5)$-C_{82} and TbNC@$C_s(6)$-C_{82} are comparable (9.0−9.1 μ_B) and agree with the theoretical limit of 9 μ_B. However, TbNC@$C_{2v}(9)$-C_{82} shows a magnetic moment that significantly exceeds the theoretical limit of 9 μ_B. This is an indication for a deviation from the noncollinear magnetic moment model.[23] The reason for the deviation of TbNC@$C_{2v}(9)$-C_{82} is unclear yet (see Supporting Information S6 for more detailed discussion).

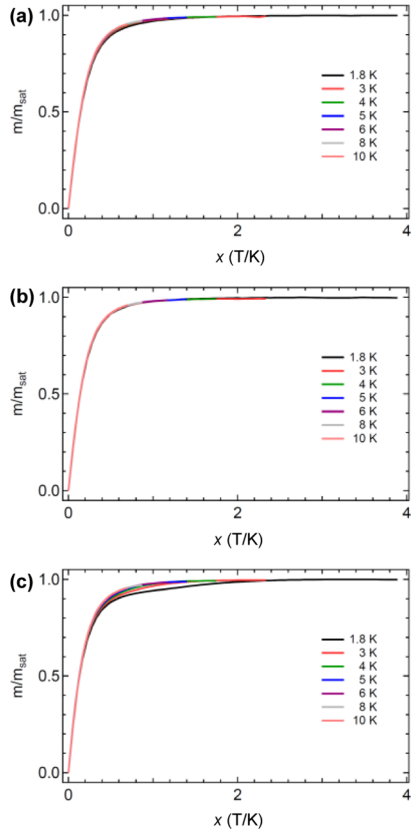

Figure 6. Magnetization of TbNC@$C_2(5)$-C_{82} (a), TbNC@$C_s(6)$-C_{82} (b) and TbNC@$C_{2v}(9)$-C_{82} (c) versus the applied field temperature quotient x. The color codes of the different temperatures are indicated. The magnetization curves scale with the applied field temperature quotient $x = \mu_0 H/T$.

However, these results reveal that the magnetic ground state of all molecules must be close to $J_z = 6$. This large J_z value is a prerequisite for single molecule magnetism. Indeed, like $HoSc_2N@C_{80}$,[24] as shown in Figure 7, the AC susceptibility identifies these three TbNC@C_{82} molecules to be field-induced single-ion magnets (SIMs).[33] In low fields ($\mu_0 H$ = 0.2 T), the AC susceptibility shows significantly temperature-dependent magnetic relaxation times. Above 4 K all three TbNC@C_{82} molecules follow the same Arrhenius-trend that indicates a demagnetization barrier between 10 and 20 K. Except for TbNC@$C_{2v}(9)$-C_{82}, the magnetic relaxation times saturate at the lowest temperatures of 1.8 K, indicating lifetimes for the quantum tunneling of the magnetization in the order of 10 to 50 ms (see Supporting Information S6). Note that, while

DOI: 10.1021/jacs.6b09329
J. Am. Chem. Soc. 2016, 138, 14764−14771

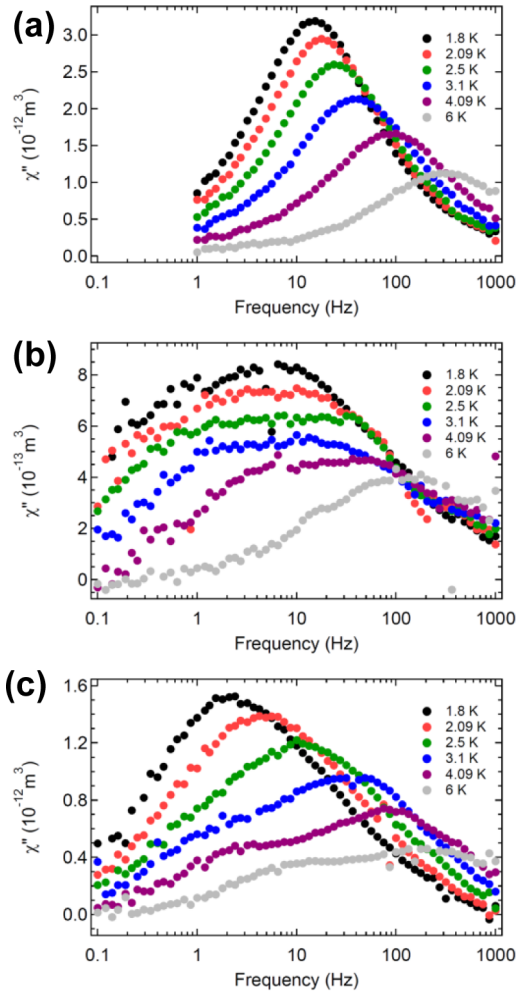

Figure 7. Imaginary part of AC susceptibility measured at different temperatures for TbNC@$C_2(5)$-C_{82} (a), TbNC@$C_s(6)$-C_{82} (b), and TbNC@$C_{2v}(9)$-C_{82} (c). $\mu_0 H = B0 + B1 \times \sin(\omega t)$, $B0$ = 200 mT, $B1$ = 0.25 mT.

TbNC@$C_2(5)$-C_{82} shows one peak for the imaginary part of the AC susceptibility in the ranges of the investigated frequencies and temperatures, the corresponding spectra for TbNC@$C_s(6)$-C_{82} and TbNC@$C_{2v}(9)$-C_{82} exhibit peak shoulders, suggesting a more complex magnetization dynamics (see Figure 7 and Supporting Information S6).

The determination of the molecular structures of these three TbNC@C_{82} molecules specifically the geometric structure of the TbNC cluster as discussed above allows a correlation between the magnetic relaxation time and atomic distance. Figure 8 shows the magnetic relaxation times of these three TbNC@C_{82} molecules for two temperatures (1.8, 6.0 K) as a function of the experimentally determined distance between the Tb ion and the closest N/C atom of the NC unit. This Tb−C(N) distance is expected to determine the strength of the ligand field that causes the lifting of the Hund degeneracy and the magnetic reversal barrier of the Tb ion. Clearly, the magnetic relaxation times measured at 1.8 K increase with the decrease of the Tb−C(N) distance. Again, noteworthy, TbNC@$C_{2v}(9)$-C_{82} shows the largest magnetic relaxation time and has the smallest Tb−C(N) distance, suggesting that the magnetic relaxation time of TbNC@C_{2n} molecule is sensitively dependent on the atomic distance in the $[TbNC]^{2+}$ cluster determined by its geometry. Intermolecular magnetic

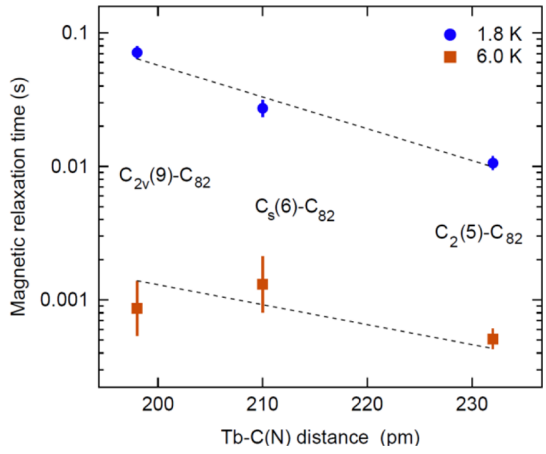

Figure 8. Magnetic relaxation times (τ) of TbNC@C_{82} ($C_2(5)$, $C_s(6)$, $C_{2v}(9)$) as a function of the distance between the Tb ion and the closest C/N atom of the NC unit. Data at 1.8 K (circles) indicate a clear decrease of the magnetization relaxation time with the increase of Tb−N(C) distance, while at 6.0 K (squares) the trend is much weaker, presumably due to thermal smearing. The dashed lines are exponential trends for TbNC@C_{82} ($C_2(5)$, $C_s(6)$, $C_{2v}(9)$), with the linear correlation coefficient between $\log(\tau)$ and the Tb−C(N) distance being −0.99 ± 0.17 and −0.69 ± 0.72 for the line at 1.8 and 6.0 K, respecitvely. Only the cage isomeric structures of TbNC@C_{82} are given in the labels for clarity.

interaction may also influence the magnetic relaxation time, while the effect is more pronounced at low temperatures.[22] At 6.0 K, where the temperature-induced demagnetization becomes dominant, the correlation trend between the magnetic relaxation time and the Tb−C(N) distance observed at 1.8 K is much weaker. This suggests that the correlation between the magnetic relaxation times and the Tb−C(N) distance is most valid in the regime of quantum tunneling of the magnetization. Accordingly we conclude that the magnetic reversal barrier of the Tb ion is different for these three TbNC@C_{82} molecules, and is affected by the isomeric structure of the fullerene cage. This systematic effect and its experimental quantification provide new insight into the underlying physics of SIMs, and highlight that magnetic relaxation time is very sensitive to the local geometric arrangement in the picometer (pm) range.

CONCLUSION

In summary, on the basis of the isolation and systematic structural studies of three isomers of TbNC@C_{82} ($C_2(5)$, $C_s(6)$, $C_{2v}(9)$), we reveal that the entrapped triangular TbNC cluster is unusual, which changes the geometric structure including Tb−N(C)/C−N bond lengths and Tb−C(N)−N(C) angle dramatically upon varying the cage isomeric structure. When the isomeric structure of C_{82} cage varies from $C_2(5)$ to $C_s(6)$ and to $C_{2v}(9)$, the triangular TbNC cluster within TbNC@C_{82} exhibits obvious distortions with the Tb−C(N)−N(C) angle varying by up to 20° and the C−N bond length changing from 0.94(5), 1.02(3) to 1.05(4) Å. The geometric structure changes of the entrapped TbNC cluster within TbNC@C_{82} ($C_2(5)$, $C_s(6)$, $C_{2v}(9)$) lead to the alternation of the magnetic relaxation times of the corresponding TbNC@C_{82} clusterfullerenes, rendering the corresponding TbNC@C_{82} as the first endohedral fullerene SIMs with geometry-dependent magnetism dictated by fullerene cage. Our discovery of the variability of the endohedral cluster and consequently tunable magnetism opens up a new avenue to

DOI: 10.1021/jacs.6b09329
J. Am. Chem. Soc. 2016, 138, 14764−14771

modulate the electronic and magnetic properties of endohedral fullerenes toward tailorable applications.

EXPERIMENTAL METHODS

Synthesis, Isolation and Spectroscopic Characterizations of TbNC@C_{82} (C_2(5), C_s(6), C_{2v}(9)). TbNC@C_{82} (C_2(5), C_s(6), C_{2v}(9)) were synthesized in a modified Krätschmer-Huffman fullerene generator by vaporizing composite graphite rods (Φ 8 × 150 mm) containing a mixture of Tb_4O_7 (99.99%) and graphite powder (molar ratio of Tb:C = 1:15) with the addition of 10 mbar N_2 into 400 mbar He as described previously.[36] To investigate the effect of TiO_2 on the formation of TbNC@C_{82}, a reference synthesis by using a mixture of Tb_4O_7, TiO_2 (99.99%) and graphite powder with a molar ratio of 1:1:15 (Tb:Ti:C) was also carried out. The as-produced soot was Soxhlet-extracted by CS_2 for 24 h, and the resulting brown-yellow solution was distilled to remove CS_2 and then immediately redissolved in toluene and subsequently passed through a 0.2 μm Telflon filter (Sartorius AG, Germany) for HPLC separation. The isolation of TbNC@C_{82} (C_2(5), C_s(6), C_{2v}(9)) was performed by multistep HPLC. The purities of the isolated TbNC@C_{82} (C_2(5), C_s(6), C_{2v}(9)) were further checked by laser desorption/ionization time-of-flight (LD-TOF) mass spectroscopic (MS) analysis (Biflex III, Bruker Daltonics Inc., Germany).

UV−vis−NIR spectra were recorded on a UV−vis−NIR 3600 spectrometer (Shimadzu, Japan) using a quartz cell of 1 mm layer thickness and 1 nm resolution with the samples dissolved in toluene.

Electrochemical Study. Electrochemical study was performed in *o*-dichlorobenzene (*o*-DCB, anhydrous, 99%, Aldrich). The supporting electrolyte was tetrabutylammonium hexafluorophosphate ($TBAPF_6$, puriss. electrochemical grade, Fluka), which was dried under reduced pressure at 340 K for 24 h and stored in glovebox prior to use. Cyclic voltammogram experiments were performed with a CHI 660 potentiostat (CH Instrument, USA) at room temperature in a glovebox. A standard three-electrode arrangement of a platinum (Pt) wire as working electrode, a platinum coil as counter electrode, and a silver wire as a pseudoreference electrode was used. In a comparison experiment, ferrocene (Fc) was added as the internal standard and all potentials are referred to the Fc/Fc^+ couple.

Magnetic Measurements. Magnetic properties were measured in a Quantum design MPMS3 Vibrating Sample Magnetometer (VSM). The samples were prepared by drop-casting from toluene solution in a plastic sample-holder. The evaporation of the solvent was increased by nitrogen flow. According to the saturation magnetization at 1.8 K, an effective moment of 4.5 μ_B (which is justified by the fit of the noncollinear magnetic moment model[23]) and the molecular mass of 1169 g/mol for TbNC@C_{82}, the sample masses of TbNC@C_2(5)-C_{82} (188 μg), TbNC@C_s(6)-C_{82} (87 μg) and TbNC@C_{2v}(9)-C_{82} (123 μg) were determined. The diamagnetic background of the capsule was subtracted from the data. In the AC measurements, an oscillating field of amplitude $\mu_0 H_{ac}$ = 25 mT was employed.

X-ray Crystallographic Studies of TbNC@C_{82} (C_s(6), C_{2v}(9)). Crystal growths of TbNC@C_{2n}·Ni^{II}(OEP)·2(C_6H_6) was accomplished by layering a solution of 1 mg Ni^{II}(OEP) (OEP = octaethylporphyrin) in 1 mL benzene over a solution of ca. 1 mg of TbNC@C_{2n} in 2 mL benzene, similar to the procedure reported recently for TbNC@C_2(5)-C_{82} (ref 36). After the two solutions diffused together over a period of one-two months, small black crystals suitable for X-ray crystallographic study formed upon a slow evaporation of benzene. X-ray diffraction data collections for the crystals of TbNC@C_{2n}·Ni^{II}(OEP)·2(C_6H_6) were carried out at 100 K on an Agilent Supernova diffractometer (Agilent Technologies, USA) with a Cu radiation (λ = 1.54178 Å). A numerical absorption correction utilizing equivalents was employed. The structure was solved by direct methods and refined using all data (based on F^2) by SHELX 2014 (ref 50). Hydrogen atoms were located in a difference map, added geometrically, and refined with a riding model. The detailed refinement parameters are listed in Supporting Information Tables S2. These data can be obtained free of charge from The Cambridge Crystallographic Data Centre with CCDC Nos. 998108 and 1000357.

Details of Computations. DFT calculations were performed first for YNC@C_{2n} using PBE functional[51] and Priroda code.[52,53] The basis set was TZ2P-quality {6,3,2}/(11s,6p,2d) for C and N atoms and SBK-type core potential with {5,5,4}/(9s,9p,8d) valence part for Y. Then, calculations for analogues TbNC@C_{2n} structure were performed at the B3LYP/def2-SVP level with Dolg's ECP basis {5,4,3}/(7s,6p,5d) for Tb (ref 54) using the Firefly code.[55]

ASSOCIATED CONTENT

Supporting Information

The Supporting Information is available free of charge on the ACS Publications website at DOI: 10.1021/jacs.6b09329.

Isolation, X-ray crystallographic analysis, Computational study, UV−vis−NIR spectroscopic analysis, Cyclic voltammograms in different scanning regions, Magnetic data of TbNC@C_{82} (C_2(5), C_s(6), C_{2v}(9)) (PDF)

X-ray crystallographic data (CIF)

X-ray crystallographic data (CIF)

AUTHOR INFORMATION

Corresponding Authors

*syxie@xmu.edu.cn

*a.popov@ifw-dresden.de

*greber@physik.uzh.ch

*sfyang@ustc.edu.cn

Notes

The authors declare no competing financial interest.

ACKNOWLEDGMENTS

We thank Prof. L.-S. Zheng (Xiamen University, China) for valuable discussions. This work was partially supported by the National Natural Science Foundation of China (NNSFC, Nos. 21132007, 21371164, 2151101074, 51572254) [to S.F.Y.], the 973 project (2014CB845601) and the NNSFC (no. U1205111) [to S.Y.X.], DFG (grant PO 1602/1-2 and DU225/31-1) and the European Research Council (ERC) under the European Union's Horizon 2020 research and innovation programme (grant agreement No 648295 "GraM3") [to A.A.P.], and the Swiss National Science Foundation (200021L_147201) within the DACH program [to T.G.]. Computational resources were provided by the Center for Information Services and High Performance Computing (ZIH) in TU Dresden. Authors thank Ulrike Nitzsche for technical assistance with computational resources in IFW Dresden.

REFERENCES

(1) Stevenson, S.; Rice, G.; Glass, T.; Harich, K.; Cromer, F.; Jordan, M. R.; Craft, J.; Hadju, E.; Bible, R.; Olmstead, M. M.; Maitra, K.; Fisher, A. J.; Balch, A. L.; Dorn, H. C. *Nature* **1999**, *401*, 55−57.

(2) Tan, Y. Z.; Xie, S. Y.; Huang, R. B.; Zheng, L. S. *Nat. Chem.* **2009**, *1*, 450−460.

(3) Popov, A. A.; Yang, S.; Dunsch, L. *Chem. Rev.* **2013**, *113*, 5989−6113.

(4) Yang, S.; Wang, C. *Endohedral Fullerenes: From Fundamentals to Applications*; World Scientific Publishing Co. Pte. Ltd.: Singapore, 2014.

(5) Wang, T.; Wang, C. *Acc. Chem. Res.* **2014**, *47*, 450−458.

(6) Zhang, J.; Stevenson, S.; Dorn, H. C. *Acc. Chem. Res.* **2013**, *46*, 1548−1557.

(7) Lu, X.; Feng, L.; Akasaka, T.; Nagase, S. *Chem. Soc. Rev.* **2012**, *41*, 7723−7760.

(8) Rodriguez-Fortea, A.; Balch, A. L.; Poblet, J. M. *Chem. Soc. Rev.* **2011**, *40*, 3551−3563.

DOI: 10.1021/jacs.6b09329
J. Am. Chem. Soc. 2016, 138, 14764−14771

(9) Yang, S.; Liu, F.; Chen, C.; Jiao, M.; Wei, T. *Chem. Commun.* **2011**, *47*, 11822−11839.
(10) Chaur, M. N.; Melin, F.; Ortiz, A. L.; Echegoyen, L. *Angew. Chem., Int. Ed.* **2009**, *48*, 7514−7538.
(11) Wang, C. R.; Kai, T.; Tomiyama, T.; Yoshida, T.; Kobayashi, Y.; Nishibori, E.; Takata, M.; Sakata, M.; Shinohara, H. *Angew. Chem., Int. Ed.* **2001**, *40*, 397−399.
(12) Zhang, J.; Bowles, F. L.; Bearden, D. W.; Ray, W. K.; Fuhrer, T.; Ye, Y.; Dixon, C.; Harich, K.; Helm, R. F.; Olmstead, M. M.; Balch, A. L.; Dorn, H. C. *Nat. Chem.* **2013**, *5*, 880−885.
(13) Lu, X.; Akasaka, T.; Nagase, S. *Acc. Chem. Res.* **2013**, *46*, 1627−1635.
(14) Stevenson, S.; Mackey, M. A.; Stuart, M. A.; Phillips, J. P.; Easterling, M. L.; Chancellor, C. J.; Olmstead, M. M.; Balch, A. L. *J. Am. Chem. Soc.* **2008**, *130*, 11844−11845.
(15) Dunsch, L.; Yang, S. F.; Zhang, L.; Svitova, A.; Oswald, S.; Popov, A. A. *J. Am. Chem. Soc.* **2010**, *132*, 5413−5421.
(16) Krause, M.; Ziegs, F.; Popov, A. A.; Dunsch, L. *ChemPhysChem* **2007**, *8*, 537−540.
(17) Wang, T. S.; Feng, L.; Wu, J. Y.; Xu, W.; Xiang, J. F.; Tan, K.; Ma, Y. H.; Zheng, J. P.; Jiang, L.; Lu, X.; Shu, C. Y.; Wang, C. R. *J. Am. Chem. Soc.* **2010**, *132*, 16362−16364.
(18) Svitova, A. L.; Ghiassi, K. B.; Schlesier, C.; Junghans, K.; Zhang, Y.; Olmstead, M. M.; Balch, A. L.; Dunsch, L.; Popov, A. A. *Nat. Commun.* **2014**, *5*, 3568.
(19) Mercado, B. Q.; Chen, N.; Rodríguez-Fortea, A.; Mackey, M. A.; Stevenson, S.; Echegoyen, L.; Poblet, J. M.; Olmstead, M. M.; Balch, A. L. *J. Am. Chem. Soc.* **2011**, *133*, 6752−6760.
(20) Cai, T.; Xu, L. S.; Anderson, M. R.; Ge, Z. X.; Zuo, T. M.; Wang, X. L.; Olmstead, M. M.; Balch, A. L.; Gibson, H. W.; Dorn, H. C. *J. Am. Chem. Soc.* **2006**, *128*, 8581−8589.
(21) Zhao, J. J.; Huang, X. M.; Jin, P.; Chen, Z. F. *Coord. Chem. Rev.* **2015**, *289*−*290*, 315−340.
(22) Westerström, R.; Dreiser, J.; Piamonteze, C.; Muntwiler, M.; Weyeneth, S.; Brune, H.; Rusponi, S.; Nolting, F.; Popov, A.; Yang, S.; Dunsch, L.; Greber, T. *J. Am. Chem. Soc.* **2012**, *134*, 9840−9843.
(23) Westerström, R.; Dreiser, J.; Piamonteze, C.; Muntwiler, M.; Weyeneth, S.; Krämer, K.; Liu, S.-X.; Decurtins, S.; Popov, A.; Yang, S.; Dunsch, L.; Greber, T. *Phys. Rev. B: Condens. Matter Mater. Phys.* **2014**, *89*, 060406.
(24) Dreiser, J.; Westerström, R.; Zhang, Y.; Popov, A. A.; Dunsch, L.; Krämer, K.; Liu, S.-X.; Decurtins, S.; Greber, T. *Chem. - Eur. J.* **2014**, *20*, 13536−13540.
(25) Westerström, R.; Uldry, A.-C.; Stania, R.; Dreiser, J.; Piamonteze, C.; Muntwiler, M.; Matsui, F.; Rusponi, S.; Brune, H.; Yang, S. F.; Popov, A.; Büchner, B.; Delley, B.; Greber, T. *Phys. Rev. Lett.* **2015**, *114*, 087201.
(26) Junghans, K.; Schlesier, C.; Kostanyan, A.; Samoylova, N. A.; Deng, Q. M.; Rosenkranz, M.; Schiemenz, S.; Westerstrçm, R.; Greber, T.; Buchner, B.; Popov, A. A. *Angew. Chem., Int. Ed.* **2015**, *54*, 13411−13415.
(27) Bogani, L.; Wernsdorfer, W. *Nat. Mater.* **2008**, *7*, 179−186.
(28) Woodruff, D. N.; Winpenny, R. E. P.; Layfield, R. A. *Chem. Rev.* **2013**, *113*, 5110−5148.
(29) Ishikawa, N.; Sugita, M.; Ishikawa, T.; Koshihara, S.-y.; Kaizu, Y. *J. Am. Chem. Soc.* **2003**, *125*, 8694−8695.
(30) Gonidec, M.; Davies, S.; McMaster, J.; Amabilino, D. B.; Veciana, J. *J. Am. Chem. Soc.* **2010**, *132*, 1756−1757.
(31) Rinehart, J. D.; Long, J. R. *Chem. Sci.* **2011**, *2*, 2078−2085.
(32) Jiang, S.-D.; Wang, B.-W.; Su, G.; Wang, Z.-M.; Gao, S. *Angew. Chem., Int. Ed.* **2010**, *49*, 7448−7451.
(33) Dreiser, J. *J. Phys.: Condens. Matter* **2015**, *27*, 183203.
(34) Ungur, L.; Chibotaru, L. F. *Phys. Chem. Chem. Phys.* **2011**, *13*, 20086−20090.
(35) Yang, S.; Chen, C.; Liu, F.; Xie, Y.; Li, F.; Jiao, M.; Suzuki, M.; Wei, T.; Wang, S.; Chen, Z.; Lu, X.; Akasaka, T. *Sci. Rep.* **2013**, *3*, 1487.
(36) Liu, F.; Wang, S.; Guan, J.; Wei, T.; Zeng, M.; Yang, S. *Inorg. Chem.* **2014**, *53*, 5201−5205.
(37) Tong, Y.-Z.; Wang, Q.-L.; Su, C.-Y.; Ma, Y.; Ren, S.; Xu, G.-F.; Yang, G.-M.; Cheng, P.; Liao, D.-Z. *CrystEngComm* **2013**, *15*, 9906−9915.
(38) Liu, J.; Knoeppel, D. W.; Liu, S.; Meyers, E. A.; Shore, S. G. *Inorg. Chem.* **2001**, *40*, 2842−2850.
(39) Entley, W. R.; Treadway, C. R.; Wilson, S. R.; Girolami, G. S. *J. Am. Chem. Soc.* **1997**, *119*, 6251−6258.
(40) Harris, K. J.; Wasylishen, R. E. *Inorg. Chem.* **2009**, *48*, 2316−2332.
(41) Stevens, P. A.; Madix, R. J.; Stohr, J. *J. Chem. Phys.* **1989**, *91*, 4338−4345.
(42) Orpen, A. G.; Brammer, L.; Allen, F. H.; Kennard, O.; Watson, D. G.; Taylor, R. *J. Chem. Soc., Dalton Trans.* **1989**, S1−S83.
(43) Wei, T.; Wang, S.; Lu, X.; Tan, Y.-Z.; Huang, J.; Liu, F.; Li, Q.; Xie, S.; Yang, S. *J. Am. Chem. Soc.* **2016**, *138*, 207−214.
(44) Wei, T.; Wang, S.; Liu, F.; Tan, Y.; Zhu, X.; Xie, S.; Yang, S. *J. Am. Chem. Soc.* **2015**, *137*, 3119−3123.
(45) Xu, W.; Feng, L.; Calvaresi, M.; Liu, J.; Liu, Y.; Niu, B.; Shi, Z.; Lian, Y.; Zerbetto, F. *J. Am. Chem. Soc.* **2013**, *135*, 4187−4190.
(46) Yang, H.; Yu, M.; Jin, H.; Liu, Z.; Yao, M.; Liu, B.; Olmstead, M. M.; Balch, A. L. *J. Am. Chem. Soc.* **2012**, *134*, 5331−5338.
(47) Zuo, T.; Xu, L.; Beavers, C. M.; Olmstead, M. M.; Fu, W.; Crawford, T. D.; Balch, A. L.; Dorn, H. C. *J. Am. Chem. Soc.* **2008**, *130*, 12992−12997.
(48) Deng, Q.; Popov, A. A. *J. Am. Chem. Soc.* **2014**, *136*, 4257−4264.
(49) Lu, X.; Slanina, Z.; Akasaka, T.; Tsuchiya, T.; Mizorogi, N.; Nagase, S. *J. Am. Chem. Soc.* **2010**, *132*, 5896−5905.
(50) Sheldrick, G. *Acta Crystallogr., Sect. C: Struct. Chem.* **2015**, *71*, 3−8.
(51) Perdew, J. P.; Burke, K.; Ernzerhof, M. *Phys. Rev. Lett.* **1996**, *77*, 3865−3868.
(52) Laikov, D. N.; Ustynuk, Y. A. *Russ. Chem. Bull.* **2005**, *54*, 820−826.
(53) Laikov, D. N. *Chem. Phys. Lett.* **1997**, *281*, 151−156.
(54) Dolg, M.; Stoll, H.; Savin, A.; Preuss, H. *Theor. Chim. Acta* **1989**, *75*, 173−194.
(55) Granovsky, A. A. *Firefly*, version 8.0.0; 2013; http://classic.chem.msu.su/gran/firefly/index.html.

DOI: 10.1021/jacs.6b09329
J. Am. Chem. Soc. 2016, 138, 14764−14771